

Analysis of the action of conventional trapped-ion entangling gates in qudit space

Pavel A. Kamenskikh,^{1,*} Nikita V. Semenin,¹ Ilia V. Zalivako,¹ Vasilii N. Smirnov,¹
Ilya A. Semerikov,^{1,2} Ksenia Yu. Khabarova,^{1,2} and Nikolay N. Kolachevsky^{1,2}

¹*P.N. Lebedev Physical Institute of the Russian Academy of Sciences, Moscow 119991, Russia*

²*Russian Quantum Center, Skolkovo, Moscow 121205, Russia*

Qudits, or multi-level quantum information carriers, present a promising path for scaling quantum computers. However, their use introduces increased complexity in quantum logic, necessitating careful control of relative phases between different qudit levels. In trapped-ion systems, entangling operations accumulate phases on specific levels that are no longer global, unlike in qubit architectures. Furthermore, the structure of multi-level gates becomes increasingly intricate with higher-dimensional Hilbert spaces. This work explores the theory of these additional entangling and non-entangling phases, accumulated in Mølmer-Sørensen and Light-shift gates. We propose methods to actively compensate for these phases, enhance gate robustness against parameter fluctuations, and simplify native gates for more efficient circuit decomposition. Our results pave the way toward the practical and scalable implementation of qudit-based quantum processors.

I. INTRODUCTION

Quantum computers have the potential to solve a variety of computational problems more efficiently than classical computers. This includes problems such as large-number factorization [1], searching through large datasets [2], solving systems of linear equations [3] and others. There are different physical platforms on which a quantum computer can be built, and the most prominent ones are superconducting circuits [4, 5], photons [6, 7], neutral atoms [8–10], trapped ions [11–13] and semiconductor quantum dots [14, 15]. Trapped ions are among the first platforms proposed [16, 17] and have demonstrated some of the highest fidelities for single-qubit gates [18] and two-qubit entangling gates [19–21]. However, the biggest challenge for real-world quantum devices based on trapped ions is scaling up the quantum register while maintaining the accuracy of quantum gates [22]. While it is possible to trap ion crystals with hundreds of particles [23], the complexity of their control, especially of their motion, prevents their usage for universal digital computers. At the moment trapped-ion universal computers usually employ ion chains no longer than 30-40 particles [24, 25]. Several methods have been proposed to solve this problem, such as photon coupling between two ion traps [26, 27] and trapped-ion QCCD (quantum charge-coupled device) architectures [28, 29].

However, while increasing the number of qubits is the conventional approach to scaling quantum computers, it is not the only way to increase the dimension of the system’s Hilbert space. An alternative is to harness a multi-level nature of ions and use more than two states in each particle for information encoding, transforming them from qubits to qudits [30]. As each d -level qudit can be treated as $\log_2(d)$ qubits [31–34] it is possible to increase an effective number of qubits in the system using the same number of ions with a rather small experi-

mental overhead. Another feature of qudits is that additional states in trapped ions can be used as ancillary levels (ancillas) in quantum circuits, allowing for reduction of the number of gates required to perform an algorithm. For example, the Toffoli gate, used in the Grover algorithm [2], can be implemented using qudits, as described in Refs. [35–38] with a significantly smaller number of entangling gates. Quantum computation using qudits has already been demonstrated on several platforms [39–43], including systems based on trapped ions, such as $^{40}\text{Ca}^+$ ions [40], $^{137}\text{Ba}^+$ ions [44] and $^{171}\text{Yb}^+$ ions [41, 43, 45].

To fully exploit the potential of qudits in gate-based applications, it is important to have a universal set of native gates, enabling one to effectively decompose quantum circuits. The supported gate set significantly affects the number of operations required to perform a given circuit, influencing the fidelity of the algorithm. Although not that pronounced in the qubit case, it becomes more and more important as the qudit dimension increases. Qudit gates can influence differently various levels of the qudits and may require many parameters for their description depending on the experimental setup, complicating the transpilation process. One example is the entangling Mølmer-Sørensen (MS) gate [46], which in the qubit case generates a $\sigma_X \otimes \sigma_X$ interaction between ions. The evolution operator corresponding to this gate also contains terms which are usually ignored as they result only in additional global phase acquired by qubits. However, when this gate is applied to qudits, they can no longer be ignored [38, 40], as well as the Stark shift imposed on spectator states (qudit states not directly involved in the gate).

In this paper, we provide a comprehensive theoretical analysis of the most common types of entangling gates, namely, Mølmer-Sørensen (MS) and Light-shift (LS), acting on trapped-ion qudits. We study the effect of these gates in the extended qudit Hilbert space, which often results in additional entangling and/or non-entangling phases acquired by various ions’ states. In contrast to previous works [40, 47] which take into ac-

* kamenskikh.pa@lebedev.ru

count interaction with only one center-of-mass (COM) motional mode, we consider interaction with multiple motional modes in the general case of a modulated laser pulse [48, 49]. It is important for control of long ion chains in universal quantum processors where closely-spaced radial modes are usually utilized for entangling. We also study ways to simplify the structure of the qudit entangling gates to optimize the process of quantum circuits decomposition. In particular, we propose pulse-shaping techniques canceling non-entangling phases acquired by spectator states during MS gate or at least making them robust to the drift of experimental parameters. For the LS gate, we propose spin-echo methods to reduce the number of entangling phases accumulated on qudit levels. We show that the proposed technique can simplify the LS gate interaction to an effective two-qubit entanglement in the case of qubit embedding. This reduction can significantly simplify the decomposition of a qubit algorithm into native qudit gates when embedded qubits are used. We note that a similar method was previously proposed in [47], however its applicability was limited to a case, where only one qudit state was experiencing a strong light shift or qudit dimension is limited to $d = 3$. Methods presented here provide a general solution for this problem. These findings are important for development of a robust and effective universal qudit quantum processor, simplification of the circuits decomposition process as well as for optimization of the calibration procedures. Our work is organized as follows. In Section II, we obtain the expressions for the qudit phases accumulated in both MS and LS gates. In Section III, we review pulse shaping methods for the MS gate that aim to make the qudit phases robust to the fluctuations of experimental parameters, such as fluctuations of laser power and motional mode frequency drifts. Section IV presents several spin-echo sequences for the LS gate designed to reduce the number of distinct entangling phases acquired by different qudit basis states. We discuss and summarise our results in Section V.

II. GENERAL DESCRIPTION OF ENTANGLING GATES ACTING ON TRAPPED-ION QUDITS

A. Mølmer-Sørensen gate

First, we analyze the $\sigma_X \otimes \sigma_X$ gate first proposed by Mølmer and Sørensen [46]. This gate involves a bichromatic electromagnetic field applied to a specific pair of ions. The bichromatic components interact with the red and blue secular motional sidebands of a transition between two qudit levels, as in Fig. 1. Without loss of generality we consider our gate acting on levels $|0\rangle$ and $|1\rangle$. The field spectral components are symmetrically detuned by μ from the carrier transition frequency, with μ selected near the ions' motional mode frequencies. Making the Lamb-Dicke approximation [50], we obtain the Hamilto-

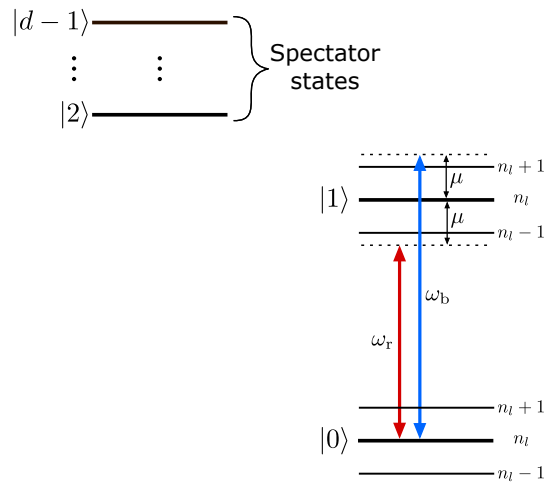


Figure 1: Schematic representation of the Mølmer-Sørensen gate, acting on levels $|0\rangle$ and $|1\rangle$. Red and blue lines represent the spectral components of the bichromatic laser beam with frequencies ω_r and ω_b . The figure also shows the motional sidebands and indicates the phonon number n_l in the l^{th} motional mode.

nian describing this interaction:

$$\hat{H}_{\text{MS}} = \sum_{l,j} \hbar \eta_{l,j} g_j(t) \left(\hat{a}_l e^{-i\omega_l t} + \hat{a}_l^\dagger e^{i\omega_l t} \right) \sigma_{\phi_S}^{(j)}, \quad (1)$$

where $g_j(t)$ is the pulse shape function for the j^{th} ion, ω_l is the frequency of the l^{th} motional mode, $\eta_{l,j}$ is the Lamb-Dicke parameter characterizing the coupling of the j^{th} ion to the l^{th} mode, \hat{a}_l and \hat{a}_l^\dagger are the annihilation and creation operators for the l^{th} mode. Phase $\phi_S^{(j)}$ and operator $\sigma_{\phi_S}^{(j)}$ are defined as

$$\sigma_{\phi_S}^{(j)} = \sigma_X^{(j)} \cos \phi_S^{(j)} + \sigma_Y^{(j)} \sin \phi_S^{(j)}, \quad \phi_S^{(j)} = \frac{\phi_r^{(j)} + \phi_b^{(j)}}{2}, \quad (2)$$

where $\phi_{r,b}^{(j)}$ is the initial phase of the red/blue components of the field for the j^{th} ion, $\sigma_X^{(j)}$ and $\sigma_Y^{(j)}$ are the standard Pauli matrices that act in the two-level subspace of the j^{th} qudit spanned by $|0\rangle$ and $|1\rangle$ (for example $\sigma_X^{(j)} = |0_j\rangle\langle 1_j| + |1_j\rangle\langle 0_j|$). The pulse function $g_j(t)$ can in the general case be expressed in terms of the Rabi frequency $\Omega_j(t)$ and the detuning $\mu(t)$ (we further consider the detuning to be the same for all ions involved):

$$g_j(t) = \Omega_j(t) \cos(\psi(t) + \phi_M^{(j)}), \quad \phi_M^{(j)} = \frac{\phi_r^{(j)} - \phi_b^{(j)}}{2}, \quad (3)$$

with the time-dependent phase $\psi(t) = \int_0^t \mu(t') dt'$.

The laser fields induce additional Stark shifts on all levels:

$$\hat{H}_{\text{AC}} = \sum_{s=0}^{d-1} \sum_j \hbar \delta_s^{\text{AC}}(t) |s_j\rangle\langle s_j|. \quad (4)$$

In practice, the Stark shifts for states $|0\rangle$ and $|1\rangle$ are calibrated to be equal, thus nullifying the differential phase accumulation between these states. This can be done, for example, by adding another off-resonant laser spectral component [51] or by introducing an imbalance in red and blue sideband amplitudes [52]. For the qudit case, these shifts, despite being equal, no longer represent a global phase and, therefore, need to be accounted for. The full Hamiltonian \hat{H} consists of the MS gate term from Eq. (1) and the Stark shift (4), so $\hat{H} = \hat{H}_{AC} + \hat{H}_{MS}$. Since these terms commute, the evolution operator can be factorized.

Phases and laser intensity for target ions can be calibrated so that $\Omega_j = \Omega$ and $\phi_S^{(j)} = \phi_M^{(j)} = 0$ for $j = 1, 2$ [53], which leads to the same pulse function for both ions $g_j(t) = g(t)$ and $\sigma_{\phi_S}^{(j)} = \sigma_X^{(j)}$. This type of operation is called the $\sigma_X \otimes \sigma_X$ gate or MS gate. Its evolution operator can be obtained using the Magnus expansion [54, 55]:

$$\hat{U}'_{MS} = \exp(\hat{A}_1 + \hat{A}_2), \quad (5)$$

where the first operator \hat{A}_1 has the form

$$\hat{A}_1 = \sum_{l,j} (\alpha_{l,j} \hat{a}_l^\dagger - \alpha_{l,j}^* \hat{a}_l) \hat{\sigma}_X^{(j)}, \quad (6)$$

the complex number $\alpha_{l,j}$ defines the position of the j^{th} ion in phase space of the l^{th} motional mode and can be written as

$$\alpha_{l,j} = -i\eta_{l,j} \int_0^\tau g(t) e^{i\omega_l t} dt. \quad (7)$$

In order to achieve ideal entanglement between ions, it is necessary to decouple the target ions from all modes, which means that

$$\alpha_{l,j} = 0 \quad \forall l, j. \quad (8)$$

Under this condition $\hat{A}_1 = 0$ at the end of the gate. This can be achieved by a proper choice of pulse function $g_j(t)$ and gate duration (this procedure is called a pulse-shaping and is discussed in more details in Appendix B). The second operator \hat{A}_2 in (5) generates the entanglement between the ions' states:

$$\hat{A}_2 = i \sum_{j,k=1}^2 \chi_{jk}^{MS} \hat{\sigma}_X^{(j)} \hat{\sigma}_X^{(k)}. \quad (9)$$

The expression for χ_{jk}^{MS} is given by

$$\chi_{jk}^{MS} = \sum_l \eta_{l,j} \eta_{l,k} \int_0^\tau dt_1 \int_0^{t_1} dt_2 g(t_1) g(t_2) \sin(\omega_l(t_1 - t_2)). \quad (10)$$

Additional details on the Magnus expansion are provided in Appendix A. The summation in Eq. (9) can be expanded as

$$\hat{A}_2 = i \left[\chi_{11}^{MS} (\sigma_X^{(1)})^2 \otimes \hat{1}_2 + \chi_{22}^{MS} \hat{1}_1 \otimes (\sigma_X^{(2)})^2 \right] + i(\chi_{12}^{MS} + \chi_{21}^{MS}) \sigma_X^{(1)} \sigma_X^{(2)}, \quad (11)$$

where $(\sigma_X^{(j)})^2 = |0_j\rangle\langle 0_j| + |1_j\rangle\langle 1_j|$ - projects onto the addressed qudit states of the j^{th} ion. The evolution operator (5) then takes the final form:

$$\hat{U}_{MS} = \exp \left(2i\chi_{12}^{MS} \sigma_X^{(1)} \sigma_X^{(2)} + i \sum_{j=1}^2 \hat{\Phi}_j \right). \quad (12)$$

The first term generates the entanglement between the target ions, so here we call $\chi_{12}^{MS} = \chi_{21}^{MS}$ - *entangling phases*. To realize a maximally entangling gate (in the qubit sense), the pulse function is usually chosen in such a way that the phase $\chi_{12}^{MS} = \chi_{21}^{MS} = \pi/8$. In the second term the operator $\hat{\Phi}_j$ changes the phases of the qudit states of the j^{th} ion:

$$\hat{\Phi}_j = \chi_{jj}^{MS} (|0_j\rangle\langle 0_j| + |1_j\rangle\langle 1_j|) + \sum_{s=0}^{d-1} \phi_s^{AC} |s_j\rangle\langle s_j|, \quad (13)$$

where $\phi_s^{AC} = -\int_0^\tau dt \delta_s^{AC}(t)$. These phases we call *non-entangling*, respectively. The effect of accumulation of the non-entangling phases on the qubit states $|0\rangle$ and $|1\rangle$ was first observed in Ref. [40]. There, the authors analyzed the special case of the MS gate in which the bichromatic field couples to a single center-of-mass motional mode, resulting in identical phases for both ions. Here we note that, in general, these non-entangling phases differ across ions when motional modes other than the center-of-mass are excited, as follows from (10). This is due to the different Lamb-Dicke factors for various ions in other modes.

B. Light-shift gate

Another common type of entangling gate for ions is a Light-Shift (LS) gate, also known as a geometric phase gate, providing a $\sigma_Z \otimes \sigma_Z$ interaction between particles. This gate is implemented using a pair of overlapping beams with different frequencies that create a so-called walking wave, as shown in Fig. 2a. The walking wave produces a light-induced Stark shift that depends on the state of the ions and on its position in the wave. As the interference pattern in the walking wave is moving, the ponderomotive force exerted on the ion from this light shift oscillates at each point. This, in turn, couples the motional modes with the electronic states. At the end of the gate the motion is again decoupled from ions' internal states while they acquire an entangling geometric

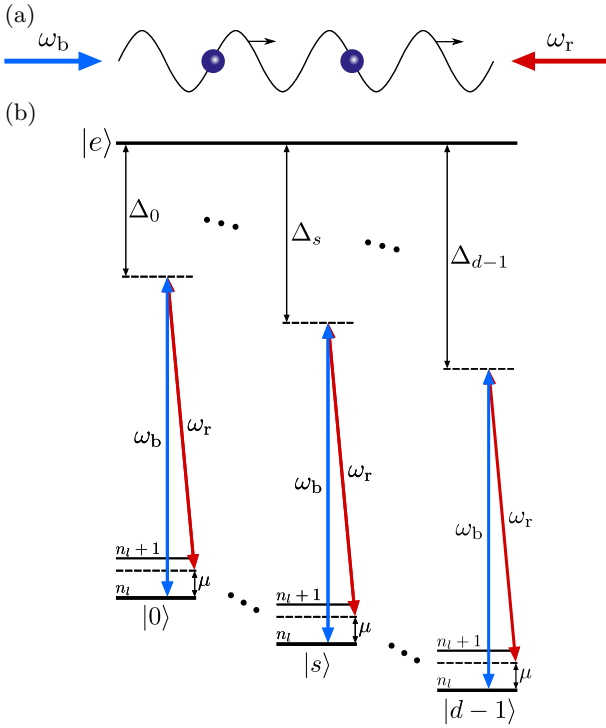


Figure 2: (a) An exemplary configuration of the LS gate, where two counter-propagating laser beams with frequencies ω_r and ω_b form a walking wave. (b) In this example state-dependent Stark shifts on qudit levels arise from their off-resonant coupling to a single auxiliary level $|e\rangle$ by these laser fields. The frequency difference between two beams is chosen close to the secular frequency ($\omega_r - \omega_b = \mu \approx \omega_l$) to excite motion. Several motional levels with different phonon numbers n_l are also depicted. The qudit states are numbered here by their proximity to the auxiliary state.

phase that depends on their initial state. The $\sigma_Z \otimes \sigma_Z$ gate was originally demonstrated by Leibfried et al. in Ref. [56].

In addition to the original scheme, there are several other configurations of the $\sigma_Z \otimes \sigma_Z$ gate, as described in Refs. [19, 23, 57]. The effective Hamiltonian is the same in all of these schemes, so we consider the most general model.

In the most general configuration of the LS gate one or several pairs of laser beams with the frequency difference $\mu(t)$ create a walking wave at the target ions' positions. The operation of the gate can be illustrated by the simple case where each qudit state is off-resonantly coupled to a single auxiliary excited state $|e\rangle$ (Fig. 2b). After adiabatic elimination [19] of all states, except ones constituting a qudit, we obtain a Hamiltonian:

$$\hat{H}(t) = \hat{H}_{AC}(t) + \hat{H}_{LS}(t), \quad (14)$$

where the first term describes the AC-Stark shift $\hat{H}_{AC} = \sum_{s=0}^{d-1} \sum_j \hbar \delta_s^{AC}(t) |s_j\rangle\langle s_j|$ which causes phase shifts on all

qudit states. The second term $\hat{H}_{LS}(t)$ describes entanglement and after the Lamb-Dicke approximation has the form

$$\hat{H}_{LS}(t) = \sum_{s=0}^{d-1} \sum_{l,j} \hbar \eta_{l,j} g_{s,j}(t) \left(\hat{a}_l e^{-i\omega_l t} + \hat{a}_l^\dagger e^{i\omega_l t} \right) |s_j\rangle\langle s_j|, \quad (15)$$

which closely resembles the MS gate Hamiltonian (1), with two crucial differences. The first one is the electronic operators, which in this case are diagonal in the computational basis. The second one is the expression for the pulse function $g_{s,j}(t)$:

$$g_{s,j}(t) = \Omega_{s,j}(t) \cos(\psi(t)), \quad (16)$$

where $\psi(t) = \int_0^t \mu(t') dt'$, and $\mu(t)$ is the time-dependent frequency difference between the laser beams. The $\Omega_{s,j}(t)$ is the light shift amplitude for a given state $|s\rangle$. For unification with Eq. (3) we further refer to it as to an effective Rabi frequency. Similarly to the MS gate, the laser power on different ions can be set in such a way that the effective Rabi frequencies are uniform across target ions, i.e. $\Omega_{s,j} = \Omega_s$ and pulse function does not depend on the ion: $g_{s,j}(t) = g_s(t)$.

The operators \hat{H}_{AC} and \hat{H}_{LS} in Eq. (14) commute, allowing the evolution operator to be factorized. We therefore obtain the evolution operator for the $\sigma_Z \otimes \sigma_Z$ -gate using the Magnus expansion. As in case of the $\sigma_X \otimes \sigma_X$ gate, the first operator \hat{A}_1 in the Magnus expansion can be set to zero by an appropriate choice of the pulse function $g_s(t)$ using the same techniques. The evolution operator for \hat{H}_{LS} can then be written as

$$\hat{U}'_{LS} = \exp \left(i \sum_{s,s'=0}^{d-1} \sum_{j,k=1}^2 \chi_{jk;ss'}^{LS} |s_j\rangle\langle s_j| \times |s'_k\rangle\langle s'_k| \right), \quad (17)$$

with the phase $\chi_{jk;ss'}^{LS}$:

$$\chi_{jk;ss'}^{LS} = \sum_l \eta_{l,j} \eta_{l,k} \int_0^\tau dt_1 \int_0^{t_1} dt_2 g_s(t_1) g_{s'}(t_2) \sin(\omega_l(t_1 - t_2)). \quad (18)$$

Although the $\sigma_Z \otimes \sigma_Z$ and $\sigma_X \otimes \sigma_X$ gates share many features, there are several important differences. The MS phases χ_{jk}^{MS} from Eq. (10) depend only on the ion indices, whereas the LS phases $\chi_{jk;ss'}^{LS}$ depend also on the qudit state. To simplify Eq. (17), we rearrange the qudit states in descending order of their light shift amplitudes, such that $|\Omega_0| \geq |\Omega_1| \geq \dots \geq |\Omega_{d-1}|$ and normalize them relative to the Ω_0 : $\Omega_s = \theta_s \Omega_0$, $|\theta_s| \leq 1$. Then, the phase from Eq. (18) becomes

$$\chi_{jk;ss'}^{LS} = \theta_s \theta_{s'} \chi_{jk}^{LS}, \quad (19)$$

where $\chi_{jk}^{LS} \equiv \chi_{jk;00}^{LS}$. The evolution operator for the full

Hamiltonian (taking into account Stark shifts) is:

$$\hat{U}_{\text{LS}} = \exp \left(2i\chi_{12}^{\text{LS}} \sum_{s,s'=0}^{d-1} \theta_s \theta_{s'} |ss'\rangle\langle ss'| + i \sum_{j=1}^2 \hat{\Phi}_j \right), \quad (20)$$

The first part generates entanglement between ions by applying different entangling phases to various qudit pair states. The second term $\hat{\Phi}_j$ describes the acquisition of non-entangling phases by states of the j^{th} ion:

$$\hat{\Phi}_j = \sum_{s=0}^{d-1} (\chi_{jj}^{\text{LS}} \theta_s^2 + \phi_s^{\text{AC}}) |s_j\rangle\langle s_j|, \quad (21)$$

where $\phi_s^{\text{AC}} = -\int_0^\tau dt \delta_s^{\text{AC}}(t)$ is the phase due to the AC-Stark shift of state $|s\rangle$.

It is important also to consider a special case of LS gate, which we call a *zero-order* LS gate, where $|\theta_{s \geq 1}| \ll 1$, meaning that only one of the states strongly interacts with the laser fields. This happens, for example, if the laser frequencies are close to some strong transition from the state $|0\rangle$ which is not the case for other states or if, due to selection rules or a specific polarization choice, the condition $\theta_s = 0$ for $s \geq 1$ is enforced. This configuration of the LS gate for qudits was considered in Ref. [47], where $|0\rangle$ is chosen from the $S_{1/2}$ term of $^{40}\text{Ca}^+$, while the remaining qudit states are selected from the $D_{5/2}$ term. As the polarizability of the $S_{1/2}$ term at 401 nm, which wavelength was used for LS gate implementation, is much higher than for a $D_{5/2}$ term, the zero-order condition was satisfied.

Under the above approximation, the evolution operator for the LS gate takes a simpler form:

$$\hat{U}_{\text{LS}}^{(0)} = \exp \left(2i\chi_{12}^{\text{LS}} |00\rangle\langle 00| + i \sum_j (\chi_{jj}^{\text{LS}} + \phi_0^{\text{AC}}) |0_j\rangle\langle 0_j| \right). \quad (22)$$

Comparing the entangling terms in evolution operators of the MS and LS gates (equations (12) and (20), respectively), MS gate acts on the $|0\rangle$ and $|1\rangle$ states only, thereby providing entanglement only in the subspace spanned by these states in both qudits. In contrast, the entangling term of the LS gate in general case acts simultaneously on all qudit states, making the structure of the entanglement much more complicated. For a more detailed analysis of the MS and LS gates in application to qudit-based quantum computing architectures, see V.

III. ROBUSTNESS TO FLUCTUATIONS OF EXPERIMENTAL PARAMETERS

Any trapped-ion entangling gate has a certain degree of sensitivity to fluctuations in the parameters of the experimental setup. Among the most prominent effects reducing the gate fidelity are laser power and phase fluctuations, nonzero temperature of the ion chain and the

heating thereof, as well as secular frequency drifts. The laser phase fluctuations and temperature have essentially the same effect for qudits as for qubits. Namely, both MS and LS gates are insensitive to the initial temperature in the first order, while the MS gate is much more susceptible to the laser phase noise than the LS gate due to its resonant nature.

Changes in secular frequencies and in laser power, however, result in a more complicated evolution in qudit systems. The reason for this is the high number of entangling and non-entangling phases for qudits, dependent on both of these parameters. A qudit MS gate has one entangling phase χ_{12}^{MS} and two non-entangling nontrivial phases $\chi_{11}^{\text{MS}}, \chi_{22}^{\text{MS}}$ which are not global, unlike their qubit counterparts. A general LS gate has $d(d-1)/2$ entangling and $d-1$ non-entangling phases (here we take into account that one of the non-entangling phases can be neglected as global). While some of non-entangling phases can be canceled similarly to the qubit case by applying additional laser fields or by tuning the balance between spectral components, the general picture for the qudit case is less robust to the fluctuations of the experimental parameters.

In both the MS and LS gates, the phases $\chi_{jk}^{\text{MS}}, \chi_{jk;ss'}^{\text{LS}}$ and $\chi_{jj}^{\text{MS}}, \chi_{jj;ss}^{\text{LS}}$ are dependent on secular frequencies and, as such, are susceptible to their drifts. Moreover, these drifts also result in residual entanglement between electronic and motional degrees of freedom of ions at the end of the gate. The latter effect is manifested in the violation of the decoupling condition (8). Therefore, the effect of frequency drifts on the gate fidelity is two-fold. Thus, a substantial effort must be made to improve the gate stability against secular frequency drifts. At the same time, changes in laser power only affect the aforementioned phases, not the decoupling condition (8), as long as it is satisfied at the end of the gate.

One of the ways to improve the robustness of qudit gates is to adopt pulse-shaping techniques widely used in qubit processors [48, 58]. They are used to reduce gates' sensitivity to the secular frequency drifts, which we further refer to as to their stabilization. Although the general type of the LS gate has too many phases to stabilize, it can still be done for the MS gate. It has only one entangling and two non-entangling phases dependent on secular frequencies. In the following subsection we show that multi-tone pulse shaping [49] can be used to stabilize both entangling and non-entangling phases with respect to secular frequency drifts. We also show that χ_{jj}^{MS} can be stabilized and set to zero at the same time. This allows one to make non-entangling phases acquired by some of the qudit states during the gate immune to not only secular frequency drifts but also to laser power fluctuations.

Stabilization of the entangling and non-entangling phases in the MS gate against experimental parameters drifts using pulse shaping

The multi-tone shaping technique discussed here simultaneously and continuously modulates the laser field's amplitude, frequency, and phase [49, 59–61]. The basic idea behind this method is to expand the pulse function $g(t)$ in a Fourier series:

$$g(t) = \sum_{p=0}^{P-1} \Omega_p \sin(\mu_p t), \quad (23)$$

where μ_p is the detuning of the p^{th} tone. The real constant coefficients Ω_p define a pulse comprising P tones with uniform frequency spacing. The straightforward way of experimental implementation of such a multi-tone MS gate is via an arbitrary waveform generator (AWG) [49].

Introducing a vector $\vec{\Omega} = (\Omega_0, \dots, \Omega_{P-1})$ we can express the phases χ_{jk}^{MS} as:

$$\chi_{jk}^{\text{MS}} = \vec{\Omega}^T \mathbf{S}_{jk} \vec{\Omega}, \quad (24)$$

where \mathbf{S}_{jk} is a symmetric matrix. To stabilize these phases against secular frequency drifts, we use the projection method [49] which projects out M eigenvectors of $\partial \mathbf{S}_{jk} / \partial \omega_l$ with the highest eigenvalue magnitudes, which correspond to the lowest robustness. Furthermore, we use the moments method [49] to stabilize the decoupling condition (8) against the aforementioned drifts as well. For a more detailed explanation of the pulse shaping and stabilization methods, see Appendix B.

For an experimental implementation of the gate, shapes that require the least laser power are favorable, due to technical limitations of the setup. Moreover, lower power causes smaller errors from carrier coupling and crosstalk between neighboring ions. We therefore optimize pulse shapes by minimizing the second norm of the amplitude vector, $\|\vec{\Omega}\|_2$, which is proportional to the mean laser power [62]:

$$\|\vec{\Omega}\|_2^2 = \sum_n \Omega_n^2 = \vec{\Omega}^T \vec{\Omega}. \quad (25)$$

Overall, we state the optimization problem as follows:

$$\begin{aligned} \min_{\vec{\Omega}} \quad & \|\vec{\Omega}\|_2^2 \\ \text{s.t.} \quad & \vec{\Omega}^T \mathbf{S}_{12} \vec{\Omega} = \chi, \\ & \vec{\Omega}^T \mathbf{S}_{jj} \vec{\Omega} = 0, \quad j = 1, 2 \\ & \mathbf{R}^T \vec{\Omega} = 0, \end{aligned} \quad (26)$$

where the matrix \mathbf{R} encompasses the stabilized decoupling condition and the projection method simultaneously. We solve this optimization problem using the sequential least squares programming algorithm (SLSQP) from the SciPy library [63].

Using SLSQP we numerically optimize pulse shapes for the multi-tone MS gate without stabilization ($M = 0$) and with $M = 5$, where M is the number of projected out eigenvectors of $\partial \mathbf{S}_{jk} / \partial \omega_l$ for each mode. It can be shown that a solution without stabilization exists for any parameter set using the multi-tone pulse-shaping method (see Appendix C). However, the usage of the projection method, used for stabilization, constrains the solution space. Consequently, for $M \neq 0$, a stabilized pulse shape cannot always be guaranteed. Nevertheless, we have verified that stabilized solutions do exist for a wide range of experimentally relevant conditions, including:

1. Arbitrary ion pairs within a chains of 3 to 20 ions
2. The secular frequencies typically employed in experiments:
 - Radial, $\nu_r \in [2, 5]$ MHz
 - Axial, $\nu_z \in [200, 700]$ kHz.

Figure 3 shows the simulated deviations

$$|\Delta \chi_{jk}| = |\chi_{jk} - \chi_{jk}^{(\text{target})}|$$

of the MS phases from their target values caused by the fluctuation in the radial center-of-mass secular frequency ν_r .

The power-optimal shapes for this plot were obtained for the following set of parameters:

- Secular frequencies $\nu_r = 3.7$ MHz and $\nu_z = 400$ kHz;
- Ion numbers: 4th and 6th in a 10-ion chain;
- Gate duration: 500 μs ;
- Target entanglement phase: $\chi = \pi/8$;
- Number of Fourier harmonics: $P = 512$.

Stabilizing all three phases χ_{12}^{MS} , χ_{11}^{MS} and χ_{22}^{MS} requires projecting out $3 \times M \times N$ vectors, where N is the number of ions in the chain. This decreases the number of degrees of freedom and, in turn, increases the power required during the gate. For a more power-efficient approach, we make use of the fact that these phases are not completely independent, but connected through the Lamb-Dicke parameters (see Eq. (10)). Therefore, stabilizing only one of them might already be sufficient. Green curves in Fig. 3 show the same phase deviations as before, but in the case when only χ_{12}^{MS} is stabilized using the projection method. This reduces the number of projected vectors to $N \times M$ and achieves performance comparable to full stabilization, making it more desirable for practical implementation.

To evaluate the power needed to drive the pulses obtained, we calculate the largest Rabi frequency achieved during the gate Ω_{max} . Table I contains the comparison between different stabilization schemes in terms of this

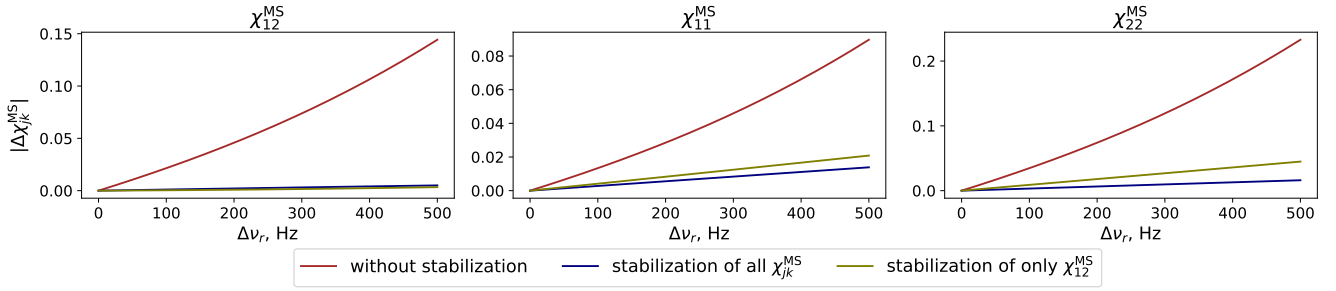


Figure 3: Sensitivity of the phases χ_{jk}^{MS} to drifts of motional modes ω_l . Fluctuations are calculated for multi-tone MS gate.

Stabilized phases χ_{jk}^{MS}	$\Omega_{\text{max}}/(2\pi)$, kHz
None	121
$\chi_{12}^{\text{MS}}, \chi_{11}^{\text{MS}}, \chi_{22}^{\text{MS}}$	431
χ_{12}^{MS}	322

Table I: Largest Rabi frequencies during the gate versus stabilization methods

parameter. Thus, conventional pulse-shaping methods developed for qubits also prove to be efficient for the MS gate acting in the qudit space in the wide range of experimental parameters.

IV. REDUCTION OF THE QUDIT LS GATE WITH SPIN-ECHO SEQUENCES

The evolution operator in Eq. (20) contains two terms: the entangling term

$$\hat{U}_{\text{LS}}^{\text{ent}} = \exp \left(i \sum_{s,s'=0}^{d-1} \phi_{ss'}^{\text{LS}} |ss'\rangle\langle ss'| \right), \quad (27)$$

where $\phi_{ss'}^{\text{LS}} = 2\chi_{12}^{\text{LS}}\theta_s\theta_{s'}$, and the non-entangling term

$$\hat{U}_{\text{LS}}^{\text{single}} = \exp \left(i(\hat{\Phi}_1 + \hat{\Phi}_2) \right). \quad (28)$$

In this section we investigate only the entangling term. The non-entangling phases are considered separately in Section IV D

In general case it contains roughly $d^2/2$ distinct entangling phases $\phi_{ss'}^{\text{LS}}$. This is quite undesirable in an experimental setup, because not only do their number grow quadratically with d , they are also not completely independent and thus difficult to control and stabilize. Moreover, even if they were controllable, usage of such a "raw" LS gate would require significant computational resources for circuits transpiling due to large number of gate parameters and its complicated structure. Lastly, for an arbitrary set of LS phases, the application of the

gate creates entanglement between all qudits' states. For some applications, it is beneficial to generate the maximal qudit entanglement in terms of, for example, the Schmidt rank [47, 64]. However, if the qudit states are used to *embed* several qubits [65, 66], a high degree of entanglement between various states after gate application becomes a burden. The more convenient gate structure in this case would be the action on two particular embedded qubits in different ions, leaving the other, spectator, qubits unperturbed. Here we investigate approaches to simplify the structure of the qudit LS gate with spin-echo sequences, allowing one to achieve such a gate behavior.

The spin-echo method is already widely used in LS gates [19, 67]. It works by splitting the whole gate into several smaller gates in such a way that in total they create the target phase shift. These smaller gates are called loops because during each of them the motional states travel along a closed trajectory on the phase diagram, leaving motion and internal degrees of freedom decoupled at the end. Spin-echo pulses are inserted between the loops to cancel residual systematic errors and suppress slow experimental parameter noise [67].

The way spin-echo can help simplify the qudit LS gate structure can be understood as follows. During each LS gate loop, a specific basis state accumulates a certain phase. Each echo pulse transfers its population to another basis state. The subsequent LS gate loop adds another phase shift, according to this new state, and so on (see fig. 4). In the end, the population is transferred

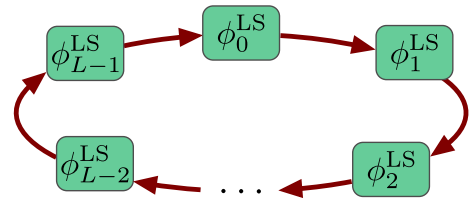


Figure 4: A general spin-echo sequence of length L . Each rectangle represents a qudit basis state, and the red arrows correspond to the echo pulses

back to the starting state, and the total phase it has acquired is equal to the sum of all entangling phases of the

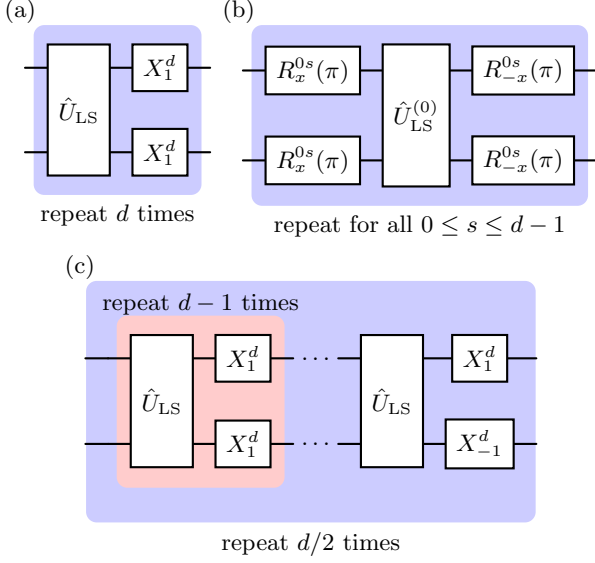


Figure 5: Spin-echo sequences for the LS gate. (a) The spin-echo sequence from Ref. [47]. (b) The spin-echo sequence that is valid for the zero-order LS gate. (c) The spin-echo sequence that can be used for a general LS gate with an even qudit dimension d .

basis states that have been "visited" by it.

The goal we pursue here is to maximally simplify the structure of the gate, so the spin-echo sequence that we seek must satisfy the following condition: the total phase $\phi_{ss'}^{\text{LS}}$ in Eq. (27) accumulated during the sequence by an initial state $|ss'\rangle$ takes the least possible number of different values among all s, s' . In this case, we refer to the resulting LS gate as the *reduced* gate. In the following, we consider the reduction of the LS gate to two phases, which is the simplest non-trivial case.

For the reduced gate with 2 phases, the entire two-qudit Hilbert space \mathbf{H} can be separated into two subspaces:

$$\mathbf{H} = \mathbf{H}_0 \oplus \mathbf{H}_1. \quad (29)$$

These spaces are spans of the basis vectors corresponding to the respective total acquired phases:

$$\phi_{ss'}^{\text{LS}} = \begin{cases} \varphi_0, & \text{if } |ss'\rangle \in \mathbf{H}_0, \\ \varphi_1, & \text{if } |ss'\rangle \in \mathbf{H}_1. \end{cases} \quad (30)$$

Obviously, for an arbitrary vector inside either of these spaces, the gate action would be the same as for the basis vectors that span them. Note that with a suitable choice of \mathbf{H}_0 and \mathbf{H}_1 the sequence, despite only featuring two phases, can still provide maximal qudit entanglement (in terms of Schmidt rank) [47]. In the following, we use the standard notation for native single-qudit rotations for trapped ions [40, 41]. The first type of gate performs a rotation of the state in the subspace spanned by the basis states $|j\rangle$ and $|k\rangle$ by angle θ around axis ϕ in the

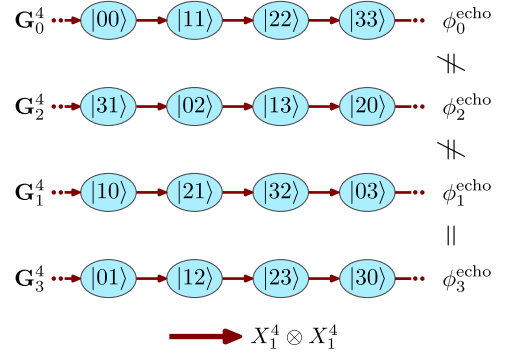


Figure 6: A scheme that shows how different states acquire the phase during the spin-echo sequence of type (a) for ququarts ($d = 4$).

equatorial plane of the Bloch sphere:

$$R_\phi^{jk}(\theta) = \exp\left(-i\frac{\theta}{2}\sigma_\phi^{jk}\right). \quad (31)$$

Here σ_ϕ^{jk} is the Pauli matrix (2) in the subspace spanned by $|j\rangle$ and $|k\rangle$. For rotations around the x -axis we use the following notations: $R_x^{jk}(\theta) := R_{\phi=0}^{jk}(\theta)$, $R_{-x}^{jk}(\theta) := R_{\phi=\pi}^{jk}(\theta)$. The second type of operation is the generalized qudit rotation around the z -axis. This is simply a phase shift applied to the state $|j\rangle$:

$$R_z^j(\theta) = \exp(i\theta|j\rangle\langle j|). \quad (32)$$

A. Type (a) sequence, zero-order case

We start our investigation from the spin-echo sequence proposed previously in Ref. [47], which we call a type (a) sequence. It is illustrated in Fig. 5a. The sequence consists of d loops, where each loop has the form $(\hat{X}_1^d \otimes \hat{X}_1^d) \cdot \hat{U}_{\text{LS}}$. The operator \hat{X}_m^d performs a cyclic permutation by m :

$$\hat{X}_m^d |j\rangle \propto |(j+m) \bmod d\rangle, \quad (33)$$

and can be realized using $O(d)$ native single-qudit rotations (See Appendix D). For convenience, we define the following subspaces:

$$\mathbf{G}_l^d = \text{span}(\{|ss'\rangle | (s-s') \bmod d = l\}). \quad (34)$$

Note that the operator $X_m^d \otimes X_m^d$ acting on $|ss'\rangle$ preserves the quantity $(s-s') \bmod d$. Therefore, the subspaces are invariant with respect to the spin-echo operators. Moreover, since each LS gate loop is identical, every logical state $|ss'\rangle \in \mathbf{G}_l^d$ spends an equal amount of time in each other logical state of its subspace, including itself (see Fig. 6). Thus, states within the same subspace acquire identical phases:

$$\phi_{ss'}^{(a)} = \phi_l^{\text{echo}}, \text{ if } |ss'\rangle \in \mathbf{G}_l^d, \quad (35)$$

where $\phi_{ss'}^{(a)}$ is the final phase acquired by the state $|ss'\rangle$ after the sequence of type (a). The phase ϕ_l^{echo} :

$$\phi_l^{\text{echo}} = \sum_s \phi_{s,(s+l)}^{\text{LS}} \pmod{d}. \quad (36)$$

Using the symmetry relation $\phi_{ss'}^{\text{LS}} = \phi_{s's}^{\text{LS}}$, we find that $\phi_{d-l}^{\text{echo}} = \phi_l^{\text{echo}}$ for all $l > 0$. Hence, after the spin-echo sequence of type (a) we obtain $\lfloor d/2 \rfloor + 1$ distinct LS phases in the general case. Therefore, for $d > 3$ the sequence of type (a) does not provide the maximum reduction of the LS gate (see Fig. 6). However, in the zero-order case (22), which took place in Ref. [47], only ϕ_{00}^{LS} is non-zero and other phases are negligible:

$$\phi_{ss'} = \begin{cases} \phi_{00}^{\text{LS}}, & \text{if } s = s' = 0, \\ 0, & \text{otherwise.} \end{cases} \quad (37)$$

Using Eq. (36):

$$\phi_l^{\text{echo}} = \begin{cases} \phi_{00}^{\text{LS}}, & \text{if } l = 0, \\ 0, & \text{otherwise.} \end{cases} \quad (38)$$

Defining $\mathbf{H}_0 = \mathbf{G}_0$, $\mathbf{H}_1 = \bigoplus_{l \neq 0} \mathbf{G}_l$, we achieve the desired LS gate reduction.

B. Type (b) sequence, zero-order case

The sequence of type (a) requires $d(d-1) = O(d^2)$ native single-qudit gates: $(d-1)$ gates for each cyclic shift times d spin-echo pulses. However, in the zero-order case, to which this scheme is anyway only applicable to, this quadratic scaling with d can be reduced using a sequence of type (b), which we propose here. The sequence has the following operator representation:

$$\hat{U}_{\text{LS}}^{(b)} = \prod_{s=0}^{d-1} R_{-x}^{0s}(\pi)^{\otimes 2} \hat{U}_{\text{LS}}^{(0)} R_x^{0s}(\pi)^{\otimes 2}, \quad (39)$$

where $R_x^{00}(\pi) = \hat{1}$. The sequence is shown in Fig. 5b. It also consists of d cycles, so the number of LS gates is the same. In the s^{th} loop we swap the population between states $|00\rangle$ and $|ss\rangle$, ensuring each $|ss\rangle$ acquires the same phase ϕ_{00}^{LS} , while leaving the phases of other states with $s \neq s'$ unaltered. After the LS gate action we reverse the swap around the $-x$ axis, so that no additional phases accumulate. The LS phases after this sequence are similar to the phases after the spin-echo sequence of type (a), i.e. $\phi^{(b)} = \phi^{(a)}$. However, the number of native single-qudit rotations reduces to $2(d-1) = O(d)$.

C. Type (c) sequence, general case for even d

In the following, we propose a spin-echo sequence that can maximally reduce the LS gate in the general case for

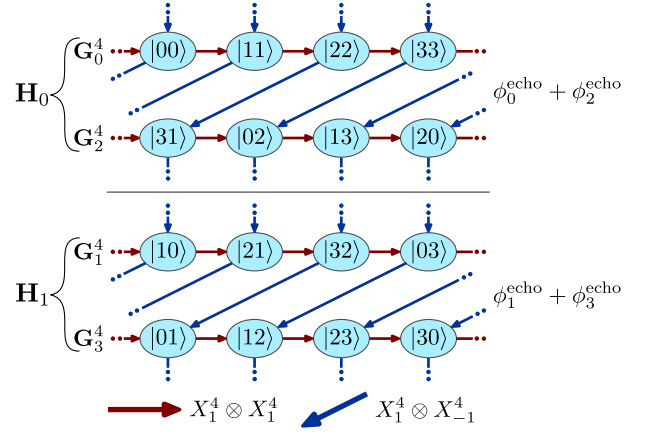


Figure 7: A schematic representation of the phase accumulation for the logical states of two qudits during the spin-echo sequence of type (c), applied to quarts ($d = 4$).

even d . First, we separate the subspaces \mathbf{G}_l^d into two different groups with even and odd indices l :

$$\mathbf{H}_0 = \bigoplus_{l-\text{even}} \mathbf{G}_l^d, \quad \mathbf{H}_1 = \bigoplus_{l-\text{odd}} \mathbf{G}_l^d. \quad (40)$$

The proposed spin-echo sequence, which we refer to as the type (c) sequence, consists of $d/2$ cycles, where each cycle has the form

$$(X_1^d \otimes X_{-1}^d) \hat{U}_{\text{LS}} \left((X_1^d \otimes X_1^d) \hat{U}_{\text{LS}} \right)^{d-1}. \quad (41)$$

The circuit is shown in Fig. 5c. To understand the principles behind this scheme, it is instructive to study the example presented in Fig. 7 for $d = 4$. The first $d-1$ operators $X_1^d \otimes X_1^d$ of the cycle shift each physical state 'along' their respective subspaces \mathbf{G}_l^d , since they are invariant. Then the last operator $X_1^d \otimes X_{-1}^d$ of the cycle shifts each \mathbf{G}_l^d 'downwards', so that $\mathbf{G}_l^d \rightarrow \mathbf{G}_{(l+2) \pmod{d}}^d$. In the end, every basis state of \mathbf{H}_0 or \mathbf{H}_1 will be visited exactly once, independent of the starting state. Therefore, the LS phase for an arbitrary state $|\psi\rangle$ in one of the subspaces will amount to one of two values:

$$\phi^{(c)}(\psi) = \begin{cases} \sum_{l-\text{even}} \phi_l^{\text{echo}}, & |\psi\rangle \in \mathbf{H}_0, \\ \sum_{l-\text{odd}} \phi_l^{\text{echo}}, & |\psi\rangle \in \mathbf{H}_1, \end{cases} \quad (42)$$

which achieves the desired reduction. Note that instead of the operator $X_1^d \otimes X_{-1}^d$ a variety of other operators can be used at the end of the cycle to shift the subspaces \mathbf{G}_l^d . That is, any operator of the form $X_{(n+2) \pmod{d}}^d \otimes X_n^d$. We select $X_1^d \otimes X_{-1}^d$, since it helps balance the number of single-qudit rotations between the two qudits, thus suppressing the accumulation of errors. Additionally, a cyclic shift with a unit step is straightforward to execute, unlike any other step (see Appendix D). Note that native rotations comprising the shifts can occasionally be

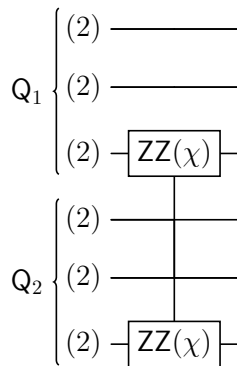


Figure 8: Operation $\text{ZZ}(\chi) := \exp(i\chi\sigma_Z \otimes \sigma_Z)$ on the last qubits embedded in different quodits ($d=8$), which is equivalent to the type (c) spin-echo sequence.

performed around the $-x$ axis, instead of $+x$, in order to compensate for over-rotation, as was done in Ref. [47]. The total number of the two-particle gates equals $d^2/2$, and the number of single qudit gates is $d^3/2$.

It can be shown (see Appendix E) that the proposed sequence directly implements a $\sigma_Z \otimes \sigma_Z$ gate between two embedded qubits in different quodits, as long as d is a power of 2 (Fig. 8). The term "directly" means that the implementation does not require any additional single-particle gates.

As a final note, we point out that the sequence of type (c) only works for even d . The reason is that, for odd d , the spaces \mathbf{H}_i are not invariant under $X_{(n+2) \bmod d}^d \otimes X_n^d$, which maps the spaces \mathbf{G}_l^d onto each other. However, a partial LS gate reduction can be achieved with $X_{(n+p) \bmod d}^d \otimes X_n^d$, where p is the smallest prime divisor of d . The spaces \mathbf{G}_l^d should then be gathered into \mathbf{H}_i by their value of l modulo p . By that construction, there will be p distinct phases.

D. Non-entangling phase compensation with spin echo

While we previously considered only the entanglement term of the LS gate, we now examine the non-entangling one (28). It is evident that the phases $\chi_{jj;ss}^{\text{LS}}$, accumulated in sequences of types (a) and (c) are all equal, since in these sequences each ion spends an equal amount of time in each of its d basis states. Therefore, these phases can be omitted as global. To see that the type (b) sequence also has this property in the zero-order approximation, we note that, for laser-induced Stark shifts, the following inequality holds: $|\delta_s^{\text{AC}}| \leq |\Omega_s|$. Hence, in the zero-order case, for which the sequence was designed, one can ignore all terms in Eq. (21) except the zero-state term:

$$\hat{\Phi}_j^{(0)} \approx (\chi_{jj}^{\text{LS}} + \phi_0^{\text{LS}}) |0_j\rangle\langle 0_j|. \quad (43)$$

Since only the $|0\rangle$ state acquires a non-negligible phase, and each ion spends an equal time in this state during the sequence, the non-entangling phases can be omitted, similarly to the cases described above. Therefore, spin-echo sequences of all types automatically provide non-entangling phase cancellation.

V. DISCUSSION AND CONCLUSION

In this paper we analyzed generalizations of MS and LS gates on trapped-ion qudits. We considered the most general case of these gates with arbitrary pulse shaping and taking into account multiple motional modes. We have shown that taking several modes into account can, for example, lead to different non-entangling phases acquired by two ions during the MS gate and studied the general form of the qudit LS gate. We also compared the robustness of these gates to fluctuations of the experimental parameters between them and with their qubit counterparts.

The simplest structure that facilitates efficient transpilation of the circuits for qubits embedded into qudits architecture and robustness is expressed by the MS and zero-order LS gates. That makes them the most suitable options for a universal qudit processor implementation. The MS gate due to its resonant nature usually requires less optical power, however is more sensitive to the laser spectral properties and is harder to use for mixed-species gates [68–75]. Moreover, the reduced number of controlled phases leads to higher fidelity of two-particle gates. For instance, the MS gate can be effectively used for implementation of a controlled-Z (CZ) gate between two embedded qubits within a pair of ququarts using a single two-particle operation [34] by setting the entangling phase $\chi_{12}^{\text{MS}} = \pi/2$. Similarly, a zero-order LS gate with $\chi_{12}^{\text{LS}} = \pi/2$ allows to implement a four-qubit CZ-gate, creating multi-qubit entanglement in a single two-particle gate [33], realizing multi-qubit entanglement. The more general forms of the LS gate, however, may offer greater utility for the quantum simulation of natively high-dimensional quantum systems.

We also demonstrated that the robustness of the MS gate can be further significantly improved using the same pulse shaping techniques that are well established for qubit processors. Moreover, we have shown that the pulse shapes optimized for the stability of the entangling phase to secular frequency drifts provide almost the same stability for the non-entangling phases. The reason for this is the interdependence of entangling and non-entangling phases, meaning that stabilizing one of the phases implicitly increases the robustness of others.

We also studied the methods for simplifying the structure of the LS gate using the spin-echo method. The spin-echo sequence of type (b) proposed in section IV B makes use of the zero-order approximation, which turns out to be a requirement for the type (a) sequence to function properly. This approximation allows for the reduced scal-

ing of the number of native single-qudit gates from $O(d^2)$ for type (a) to $O(d)$ for type (b).

The spin-echo sequence of type (c) proposed in section IV C has the $O(d^2)$ scaling on the required number of LS gates. Despite this method looking considerably less appealing than the type (a) method, which only requires $O(d)$ two-qudit gates, we believe that, in the most general case, no spin-echo sequence that reduces the number of distinct two-qudit phases to two (or any fixed number independent of d) can have better scaling. Our reasoning is based on the following. There are $O(d^2)$ LS phases $\phi_{ss'}$, and gate reduction ultimately comes down to distributing these phases among a fixed number of "boxes", with the sum of all phases in each box being the total accumulated spin-echo phase. The number of phases in each box grows quadratically with d , since they contain a fixed fraction of the entire set of phases. To perform the sequence, one has to move a specific basis state across the states in a box while performing LS gates on each of those intermediate states. Thus, the number of LS gates should also scale quadratically. This argument is further reinforced by the result obtained in Ref. [33], where the number of two-particle gates needed to realize a controlled-Z gate on embedded qubits also grows quadratically with the qudit dimension. A single-qudit

cyclic shift (or any permutation in general) requires $O(d)$ native gates, therefore, the scaling for the native gate number cannot be better than d times the scaling for the number of LS gates, that is, $O(d^3)$. The only exception is the zero-order case, for which there are d non-zero LS phases, and so the type (a) and (b) sequences have the $O(d)$ scaling. Therefore, if possible, one should try to preemptively eliminate as many phases as possible by choosing a more convenient qudit space, suitable polarizations, etc. to avoid the need of too many two-particle gates.

In general, we believe that the methods studied in this work should be applicable in a variety of different cases, depending on the physical properties of the ion and the technical limitations of a specific experimental setup. When using qudits, one should pay close attention to the nontrivial qudit phases and make corresponding changes to the conventional two-qubit entangling gate design.

ACKNOWLEDGEMENTS

This research was supported by the Russian State Corporation "Rosatom" within the Roadmap on Quantum Computing, Contract No. 868/1653-D dated 21 August 2025.

-
- [1] P. W. Shor, Algorithms for quantum computation: Discrete logarithms and factoring, in *Proceedings 35th Annual Symposium on Foundations of Computer Science* (Ieee, 1994) pp. 124–134.
- [2] L. K. Grover, A fast quantum mechanical algorithm for database search, in *Proceedings of the Twenty-Eighth Annual ACM Symposium on Theory of Computing - STOC '96* (ACM Press, Philadelphia, Pennsylvania, United States, 1996) pp. 212–219.
- [3] A. W. Harrow, A. Hassidim, and S. Lloyd, Quantum Algorithm for Linear Systems of Equations, *Physical Review Letters* **103**, 150502 (2009).
- [4] Y. Wu, W.-S. Bao, S. Cao, F. Chen, M.-C. Chen, X. Chen, T.-H. Chung, H. Deng, Y. Du, D. Fan, M. Gong, C. Guo, C. Guo, S. Guo, L. Han, L. Hong, H.-L. Huang, Y.-H. Huo, L. Li, N. Li, S. Li, Y. Li, F. Liang, C. Lin, J. Lin, H. Qian, D. Qiao, H. Rong, H. Su, L. Sun, L. Wang, S. Wang, D. Wu, Y. Xu, K. Yan, W. Yang, Y. Yang, Y. Ye, J. Yin, C. Ying, J. Yu, C. Zha, C. Zhang, H. Zhang, K. Zhang, Y. Zhang, H. Zhao, Y. Zhao, L. Zhou, Q. Zhu, C.-Y. Lu, C.-Z. Peng, X. Zhu, and J.-W. Pan, Strong Quantum Computational Advantage Using a Superconducting Quantum Processor, *Physical Review Letters* **127**, 180501 (2021).
- [5] F. Arute, K. Arya, R. Babbush, D. Bacon, J. C. Bardin, R. Barends, R. Biswas, S. Boixo, F. G. Brandao, and D. A. Buell, Quantum supremacy using a programmable superconducting processor, *Nature* **574**, 505 (2019).
- [6] H.-S. Zhong, H. Wang, Y.-H. Deng, M.-C. Chen, L.-C. Peng, Y.-H. Luo, J. Qin, D. Wu, X. Ding, Y. Hu, P. Hu, X.-Y. Yang, W.-J. Zhang, H. Li, Y. Li, X. Jiang, L. Gan, G. Yang, L. You, Z. Wang, L. Li, N.-L. Liu, C.-Y. Lu, and J.-W. Pan, Quantum computational advantage using photons, *Science* **370**, 1460 (2020).
- [7] L. S. Madsen, F. Laudenbach, M. F. Askarani, F. Rortais, T. Vincent, J. F. Bulmer, F. M. Miatto, L. Neuhaus, L. G. Helt, and M. J. Collins, Quantum computational advantage with a programmable photonic processor, *Nature* **606**, 75 (2022).
- [8] S. Ebadi, T. T. Wang, H. Levine, A. Keesling, G. Semeghini, A. Omran, D. Bluvstein, R. Samajdar, H. Pichler, and W. W. Ho, Quantum phases of matter on a 256-atom programmable quantum simulator, *Nature* **595**, 227 (2021).
- [9] L. Henriot, L. Beguin, A. Signoles, T. Lahaye, A. Browaeys, G.-O. Reymond, and C. Jurczak, Quantum computing with neutral atoms, *Quantum* **4**, 327 (2020).
- [10] D. Bluvstein, S. J. Evered, A. A. Geim, S. H. Li, H. Zhou, T. Manovitz, S. Ebadi, M. Cain, M. Kalinowski, and D. Hangleiter, Logical quantum processor based on reconfigurable atom arrays, *Nature* **626**, 58 (2024).
- [11] S. Debnath, N. M. Linke, C. Figgatt, K. A. Landsman, K. Wright, and C. Monroe, Demonstration of a small programmable quantum computer with atomic qubits, *Nature* **536**, 63 (2016).
- [12] J. Zhang, G. Pagano, P. W. Hess, A. Kyprianidis, P. Becker, H. Kaplan, A. V. Gorshkov, Z.-X. Gong, and C. Monroe, Observation of a many-body dynamical phase transition with a 53-qubit quantum simulator, *Nature* **551**, 601 (2017).
- [13] S. A. Moses, C. H. Baldwin, M. S. Allman, R. Ancona, L. Ascarrunz, C. Barnes, J. Bartolotta, B. Bjork,

- P. Blanchard, M. Bohn, J. G. Bohnet, N. C. Brown, N. Q. Burdick, W. C. Burton, S. L. Campbell, J. P. Campora, C. Carron, J. Chambers, J. W. Chan, Y. H. Chen, A. Chernoguzov, E. Chertkov, J. Colina, J. P. Curtis, R. Daniel, M. DeCross, D. Deen, C. Delaney, J. M. Dreiling, C. T. Ertsgaard, J. Esposito, B. Estey, M. Fabrikant, C. Figgatt, C. Foltz, M. Foss-Feig, D. Francois, J. P. Gaebler, T. M. Gatterman, C. N. Gilbreth, J. Giles, E. Glynn, A. Hall, A. M. Hankin, A. Hansen, D. Hayes, B. Higashi, I. M. Hoffman, B. Horning, J. J. Hout, R. Jacobs, J. Johansen, L. Jones, J. Karcz, T. Klein, P. Lauria, P. Lee, D. Liefer, S. T. Lu, D. Lucchetti, C. Lytle, A. Malm, M. Matheny, B. Mathewson, K. Mayer, D. B. Miller, M. Mills, B. Neyenhuis, L. Nugent, S. Olson, J. Parks, G. N. Price, Z. Price, M. Pugh, A. Ransford, A. P. Reed, C. Roman, M. Rowe, C. Ryan-Anderson, S. Sanders, J. Sedlacek, P. Shevchuk, P. Siegfried, T. Skripka, B. Spaun, R. T. Sprenkle, R. P. Stutz, M. Swallows, R. I. Tobey, A. Tran, T. Tran, E. Vogt, C. Volin, J. Walker, A. M. Zolot, and J. M. Pino, A Race-Track Trapped-Ion Quantum Processor, *Physical Review X* **13**, 041052 (2023).
- [14] A. Noiri, K. Takeda, T. Nakajima, T. Kobayashi, A. Sammak, G. Scappucci, and S. Tarucha, Fast universal quantum gate above the fault-tolerance threshold in silicon, *Nature* **601**, 338 (2022).
- [15] X. Xue, M. Russ, N. Samkharadze, B. Undseth, A. Sammak, G. Scappucci, and L. M. Vandersypen, Quantum logic with spin qubits crossing the surface code threshold, *Nature* **601**, 343 (2022).
- [16] C. Monroe, D. M. Meekhof, B. E. King, W. M. Itano, and D. J. Wineland, Demonstration of a Fundamental Quantum Logic Gate, *Physical Review Letters* **75**, 4714 (1995).
- [17] J. I. Cirac and P. Zoller, Quantum Computations with Cold Trapped Ions, *Physical Review Letters* **74**, 4091 (1995).
- [18] M. C. Smith, A. D. Leu, K. Miyanishi, M. F. Gely, and D. M. Lucas, Single-Qubit Gates with Errors at the 10⁻⁷ Level, *Physical Review Letters* **134**, 230601 (2025).
- [19] C. H. Baldwin, B. J. Bjork, M. Foss-Feig, J. P. Gaebler, D. Hayes, M. G. Kokish, C. Langer, J. A. Sedlacek, D. Stack, and G. Vittorini, High-fidelity light-shift gate for clock-state qubits, *Physical Review A* **103**, 012603 (2021).
- [20] C. M. Löschnauer, J. M. Toba, A. C. Hughes, S. A. King, M. A. Weber, R. Srinivas, R. Matt, R. Nourshargh, D. T. C. Allcock, C. J. Ballance, C. Matthiesen, M. Malinowski, and T. P. Harty, Scalable, high-fidelity all-electronic control of trapped-ion qubits (2024), [arXiv:2407.07694 \[physics, physics:quant-ph\]](https://arxiv.org/abs/2407.07694).
- [21] A. Hughes, R. Srinivas, C. Löschnauer, H. Knaack, R. Matt, C. Ballance, M. Malinowski, T. Harty, and R. Sutherland, Trapped-ion two-qubit gates with 99.99% fidelity without ground-state cooling, *arXiv preprint arXiv:2510.17286* (2025).
- [22] C. D. Bruzewicz, J. Chiaverini, R. McConnell, and J. M. Sage, Trapped-ion quantum computing: Progress and challenges, *Applied Physics Reviews* **6** (2019).
- [23] S.-A. Guo, Y.-K. Wu, J. Ye, L. Zhang, W.-Q. Lian, R. Yao, Y. Wang, R.-Y. Yan, Y.-J. Yi, and Y.-L. Xu, A site-resolved two-dimensional quantum simulator with hundreds of trapped ions, *Nature*, 1 (2024).
- [24] L. Cheng, S.-C. Liu, L.-Y. Peng, and Q. Gong, Crosstalk suppression of parallel gates for fault-tolerant quantum computation with trapped ions via optical tweezers, *Physical Review Applied* **22**, 034021 (2024).
- [25] I. Pogorelov, T. Feldker, Ch. D. Marciniak, L. Postler, G. Jacob, O. Krieglsteiner, V. Podlesnic, M. Meth, V. Negnevitsky, M. Stadler, B. Höfer, C. Wächter, K. Lakhmanskiy, R. Blatt, P. Schindler, and T. Monz, Compact Ion-Trap Quantum Computing Demonstrator, *PRX Quantum* **2**, 020343 (2021).
- [26] C. Monroe and J. Kim, Scaling the Ion Trap Quantum Processor, *Science* **339**, 1164 (2013).
- [27] D. Main, P. Drmota, D. P. Nadlinger, E. M. Ainley, A. Agrawal, B. C. Nichol, R. Srinivas, G. Aranedá, and D. M. Lucas, Distributed quantum computing across an optical network link, *Nature*, 1 (2025).
- [28] D. Kielpinski, C. Monroe, and D. J. Wineland, Architecture for a large-scale ion-trap quantum computer, *Nature* **417**, 709 (2002).
- [29] J. M. Pino, J. M. Dreiling, C. Figgatt, J. P. Gaebler, S. A. Moses, M. S. Allman, C. H. Baldwin, M. Foss-Feig, D. Hayes, and K. Mayer, Demonstration of the trapped-ion quantum CCD computer architecture, *Nature* **592**, 209 (2021).
- [30] Y. Wang, Z. Hu, B. C. Sanders, and S. Kais, Qudits and high-dimensional quantum computing, *Frontiers in Physics* **8**, 589504 (2020).
- [31] A. R. Kessel' and V. L. Ermakov, Multiqubit spin, *Journal of Experimental and Theoretical Physics Letters* **70**, 61 (1999).
- [32] A. R. Kessel and N. M. Yakovleva, Implementation schemes in NMR of quantum processors and the Deutsch-Jozsa algorithm by using virtual spin representation, *Physical Review A* **66**, 062322 (2002).
- [33] A. S. Nikolaeva, E. O. Kiktenko, and A. K. Fedorov, Efficient realization of quantum algorithms with qudits, *EPJ Quantum Technology* **11**, 43 (2024).
- [34] A. S. Nikolaeva, E. O. Kiktenko, and A. K. Fedorov, Universal quantum computing with qubits embedded in trapped-ion qudits, *Physical Review A* **109**, 022615 (2024).
- [35] T. C. Ralph, K. J. Resch, and A. Gilchrist, Efficient Toffoli gates using qudits, *Physical Review A* **75**, 022313 (2007).
- [36] A. Fedorov, L. Steffen, M. Baur, M. P. da Silva, and A. Wallraff, Implementation of a Toffoli gate with superconducting circuits, *Nature* **481**, 170 (2012).
- [37] A. S. Nikolaeva, E. O. Kiktenko, and A. K. Fedorov, Decomposing the generalized Toffoli gate with qutrits, *Physical Review A* **105**, 032621 (2022).
- [38] A. S. Nikolaeva, I. V. Zalivako, A. S. Borisenko, N. V. Semenina, K. P. Galstyan, A. E. Korolkov, E. O. Kiktenko, K. Y. Khabarova, I. A. Semerikov, A. K. Fedorov, and N. N. Kolachevsky, Scalable Improvement of the Generalized Toffoli Gate Realization Using Trapped-Ion-Based Qutrits, *Physical Review Letters* **135**, 060601 (2025).
- [39] A. D. Hill, M. J. Hodson, N. Didier, and M. J. Reagor, Realization of arbitrary doubly-controlled quantum phase gates (2021), [arXiv:2108.01652 \[quant-ph\]](https://arxiv.org/abs/2108.01652).
- [40] M. Ringbauer, M. Meth, L. Postler, R. Stricker, R. Blatt, P. Schindler, and T. Monz, A universal qudit quantum processor with trapped ions, *Nature Physics* **18**, 1053 (2022).

- [41] M. A. Aksenov, I. V. Zalivako, I. A. Semerikov, A. S. Borisenko, N. V. Semenin, P. L. Sidorov, A. K. Fedorov, K. Yu. Khabarova, and N. N. Kolachevsky, Realizing quantum gates with optically addressable Yb + 171 ion qudits, *Physical Review A* **107**, 052612 (2023).
- [42] A. S. Kazmina, I. V. Zalivako, A. S. Borisenko, N. A. Nemkov, A. S. Nikolaeva, I. A. Simakov, A. V. Kuznetsova, E. Y. Egorova, K. P. Galstyan, N. V. Semenin, A. E. Korolkov, I. N. Moskalenko, N. N. Abramov, I. S. Besedin, D. A. Kalacheva, V. B. Lubanov, A. N. Bolgar, E. O. Kiktenko, K. Y. Khabarova, A. Galda, I. A. Semerikov, N. N. Kolachevsky, N. Maleeva, and A. K. Fedorov, Demonstration of a parity-time-symmetry-breaking phase transition using superconducting and trapped-ion qutrits, *Physical Review A* **109**, 032619 (2024).
- [43] I. V. Zalivako, A. S. Nikolaeva, A. S. Borisenko, A. E. Korolkov, P. L. Sidorov, K. P. Galstyan, N. V. Semenin, V. N. Smirnov, M. A. Aksenov, K. M. Makushin, E. O. Kiktenko, A. K. Fedorov, I. A. Semerikov, K. Y. Khabarova, and N. N. Kolachevsky, Towards multiqubit quantum processor based on a $^{171}\text{Yb}^{+}$ ion string: Realizing basic quantum algorithms, *Quantum Reports* **7**, 19 (2025), [arXiv:2402.03121 \[quant-ph\]](https://arxiv.org/abs/2402.03121).
- [44] P. J. Low, B. White, and C. Senko, Control and readout of a 13-level trapped ion qudit, *npj Quantum Information* **11**, 85 (2025).
- [45] J. Bian, T. Liu, M. Ding, Q. Lao, H. Zhang, X. Rao, P. Lu, and L. Luo, Architecture of a scalable universal quantum processor by encoding two qubits on electron and nuclear spins in a trapped ion, *New Journal of Physics* **28**, 014509 (2026).
- [46] K. Mølmer and A. Sørensen, Multiparticle Entanglement of Hot Trapped Ions, *Physical Review Letters* **82**, 1835 (1999).
- [47] P. Hrmo, B. Wilhelm, L. Gerster, M. W. van Mourik, M. Huber, R. Blatt, P. Schindler, T. Monz, and M. Ringbauer, Native qudit entanglement in a trapped ion quantum processor, *Nature Communications* **14**, 2242 (2023).
- [48] T. Choi, S. Debnath, T. A. Manning, C. Figgatt, Z.-X. Gong, L.-M. Duan, and C. Monroe, Optimal Quantum Control of Multimode Couplings between Trapped Ion Qubits for Scalable Entanglement, *Physical Review Letters* **112**, 190502 (2014).
- [49] R. Blümel, N. Grzesiak, N. Pienti, K. Wright, and Y. Nam, Power-optimal, stabilized entangling gate between trapped-ion qubits, *npj Quantum Information* **7**, 147 (2021).
- [50] D. Leibfried, R. Blatt, C. Monroe, and D. Wineland, Quantum dynamics of single trapped ions, *Reviews of Modern Physics* **75**, 281 (2003).
- [51] J. Franke, S. R. Muleady, R. Kaubruegger, F. Kranzl, R. Blatt, A. M. Rey, M. K. Joshi, and C. F. Roos, Quantum-enhanced sensing on optical transitions through finite-range interactions, *Nature* **621**, 740 (2023).
- [52] G. Kirchmair, J. Benhelm, F. Zähringer, R. Gerritsma, C. F. Roos, and R. Blatt, Deterministic entanglement of ions in thermal states of motion, *New Journal of Physics* **11**, 023002 (2009).
- [53] L. Gerster, F. Martínez-García, P. Hrmo, M. W. Van Mourik, B. Wilhelm, D. Vodola, M. Müller, R. Blatt, P. Schindler, and T. Monz, Experimental Bayesian Calibration of Trapped-Ion Entangling Operations, *PRX Quantum* **3**, 020350 (2022).
- [54] S. Blanes, F. Casas, J.-A. Oteo, and J. Ros, The Magnus expansion and some of its applications, *Physics reports* **470**, 151 (2009).
- [55] W. Magnus, On the exponential solution of differential equations for a linear operator, *Communications on Pure and Applied Mathematics* **7**, 649 (1954).
- [56] D. Leibfried, B. DeMarco, V. Meyer, D. Lucas, M. Barrett, J. Britton, W. M. Itano, B. Jelenković, C. Langer, and T. Rosenband, Experimental demonstration of a robust, high-fidelity geometric two ion-qubit phase gate, *Nature* **422**, 412 (2003).
- [57] L. Aolita, K. Kim, J. Benhelm, C. F. Roos, and H. Häffner, High-fidelity ion-trap quantum computing with hyperfine clock states, *Physical Review A* **76**, 040303 (2007).
- [58] V. M. Schäfer, C. J. Ballance, K. Thirumalai, L. J. Stephenson, T. G. Ballance, A. M. Steane, and D. M. Lucas, Fast quantum logic gates with trapped-ion qubits, *Nature* **555**, 75 (2018).
- [59] F. Haddadfarshi and F. Mintert, High fidelity quantum gates of trapped ions in the presence of motional heating, *New Journal of Physics* **18**, 123007 (2016).
- [60] Y. Shapira, R. Shaniv, T. Manovitz, N. Akerman, L. Peleg, L. Gazit, R. Ozeri, and A. Stern, Theory of robust multiqubit nonadiabatic gates for trapped ions, *Physical Review A* **101**, 032330 (2020).
- [61] A. E. Webb, S. C. Webster, S. Collingbourne, D. Breaud, A. M. Lawrence, S. Weidt, F. Mintert, and W. K. Hensinger, Resilient Entangling Gates for Trapped Ions, *Physical Review Letters* **121**, 180501 (2018).
- [62] D. F. James, *Quantum Dynamics of Cold Trapped Ions with Application to Quantum Computation*, Tech. Rep. (1998).
- [63] P. Virtanen, R. Gommers, T. E. Oliphant, M. Haberland, T. Reddy, D. Cournapeau, E. Burovski, P. Peterson, W. Weckesser, and J. Bright, SciPy 1.0: Fundamental algorithms for scientific computing in Python, *Nature methods* **17**, 261 (2020).
- [64] G. K. Brennen, S. S. Bullock, and D. P. O’Leary, *Efficient Circuits for Exact-Universal Computations with Qudits* (2005), [arXiv:quant-ph/0509161](https://arxiv.org/abs/quant-ph/0509161).
- [65] A. K. Fedorov, N. Gisin, S. M. Belousov, and A. I. Lvovsky, Quantum computing at the quantum advantage threshold: A down-to-business review (2022), [arXiv:2203.17181 \[physics, physics:quant-ph\]](https://arxiv.org/abs/2203.17181).
- [66] E. O. Kiktenko, A. S. Nikolaeva, and A. K. Fedorov, *Colloquium* : Qudits for decomposing multiqubit gates and realizing quantum algorithms, *Reviews of Modern Physics* **97**, 021003 (2025).
- [67] C. F. Roos, Ion trap quantum gates with amplitude-modulated laser beams, *New Journal of Physics* **10**, 013002 (2008).
- [68] B. C. Sawyer and K. R. Brown, Wavelength-insensitive, multispecies entangling gate for group-2 atomic ions, *Physical Review A* **103**, 022427 (2021).
- [69] A. C. Hughes, V. M. Schäfer, K. Thirumalai, D. P. Nadlinger, S. R. Woodrow, D. M. Lucas, and C. J. Ballance, Benchmarking a High-Fidelity Mixed-Species Entangling Gate, *Physical Review Letters* **125**, 080504 (2020).
- [70] C. J. Ballance, V. M. Schäfer, J. P. Home, D. J. Szwer, S. C. Webster, D. T. C. Allcock, N. M. Linke, T. P. Harty, D. P. L. Aude Craik, and D. N. Stacey, Hybrid quantum

logic and a test of Bell's inequality using two different atomic isotopes, *Nature* **528**, 384 (2015).

- [71] I. V. Inlek, C. Crocker, M. Lichtman, K. Sosnova, and C. Monroe, Multispecies Trapped-Ion Node for Quantum Networking, *Physical Review Letters* **118**, 250502 (2017).
- [72] T. R. Tan, J. P. Gaebler, Y. Lin, Y. Wan, R. Bowler, D. Leibfried, and D. J. Wineland, Multi-element logic gates for trapped-ion qubits, *Nature* **528**, 380 (2015).
- [73] V. Negnevitsky, M. Marinelli, K. K. Mehta, H.-Y. Lo, C. Flühmann, and J. P. Home, Repeated multi-qubit readout and feedback with a mixed-species trapped-ion

register, *Nature* **563**, 527 (2018).

- [74] C. D. Bruzewicz, R. McConnell, J. Stuart, J. M. Sage, and J. Chiaverini, Dual-species, multi-qubit logic primitives for Ca+/Sr+ trapped-ion crystals, *npj Quantum Information* **5**, 102 (2019).
- [75] Y. Wan, D. Kienzler, S. D. Erickson, K. H. Mayer, T. R. Tan, J. J. Wu, H. M. Vasconcelos, S. Glancy, E. Knill, D. J. Wineland, A. C. Wilson, and D. Leibfried, Quantum gate teleportation between separated qubits in a trapped-ion processor, *Science* **364**, 875 (2019).

Appendix A: Magnus expansion for MS and LS gates. Decoupling condition.

In our work we often use the Magnus expansion [55] to obtain the evolution operator of time dependent hamiltonian $\hat{H}(t)$:

$$\hat{U} = \exp\left(\sum_{k=1}^{\infty} \hat{A}_k(t)\right), \quad (\text{A1})$$

where the first two operators are

$$\hat{A}_1 = -\frac{i}{\hbar} \int_0^t dt_1 \hat{H}(t_1) \quad (\text{A2})$$

$$\hat{A}_2 = \frac{1}{2} \left(\frac{i}{\hbar}\right)^2 \int_0^t dt_1 \int_0^{t_1} dt_2 [\hat{H}(t_1), \hat{H}(t_2)] \quad (\text{A3})$$

Note, that the Magnus expansion is used both for the $\sigma_X \otimes \sigma_X$ and the $\sigma_Z \otimes \sigma_Z$ gates, as their Hamiltonians have a similar structure (compare Eqs. (1) and (14)). For such Hamiltonians the Magnus expansion (A1) terminates at the second order, since all higher-order terms vanish due to the commutation relations $[\hat{a}_l, [\hat{a}_l, \hat{a}_l^\dagger]] = [\hat{a}_l^\dagger, [\hat{a}_l, \hat{a}_l^\dagger]] = 0$.

This yields explicit expressions for the Magnus operators \hat{A}_1 and \hat{A}_2 for the MS gate that are used in the main text. We first derive the \hat{A}_1 :

$$\hat{A}_1 = \sum_{l,j} \left(\alpha_{l,j} \hat{a}_l^\dagger - \alpha_{l,j}^* \hat{a}_l \right) \hat{\sigma}_X^{(j)}, \quad (\text{A4})$$

where the complex coefficients $\alpha_{l,j}$ define the displacement of the l^{th} motional mode and j^{th} ion. This parameters depend on the pulse function $g(t)$ as was shown in Eq. (7). Using linear transformations we can rewrite the system (7):

$$\int_0^\tau g(t) \cos\left[\omega_l \left(\frac{\tau}{2} - t\right)\right] dt = 0, \quad (\text{A5})$$

$$\int_0^\tau g(t) \sin\left[\omega_l \left(\frac{\tau}{2} - t\right)\right] dt = 0, \quad \forall l = 1, \dots, N. \quad (\text{A6})$$

For an anti-symmetric pulse function $g(t)$, satisfying $g(\tau - t) = -g(t)$ about the gate midpoint, the equations in (A5) vanish identically. So only remaining equations (A6) need to be solved. The second operator of the MS gate (9) given in the main text follows directly from (A3) when evaluated for the Hamiltonian of the MS gate (1).

Similarly, we use Magnus expansion for LS gate and obtain the first operator \hat{A}_1 :

$$\hat{A}_1 = \sum_{s=0}^{d-1} \sum_{l,j} \left(\alpha_{l,j,s} \hat{a}_l^\dagger - \alpha_{l,j,s}^* \hat{a}_l \right) |s_j\rangle\langle s_j|, \quad (\text{A7})$$

where the $\alpha_{l,j,s}$ defines the displacement of the l^{th} motional mode and the $|s\rangle$ state of the j^{th} qudit. The $\alpha_{l,j,s}$ has the form:

$$\alpha_{l,j,s} = -i\eta_{l,j} \int_0^\tau \Omega_s(t) \cos(\mu t) e^{i\omega_l t} dt. \quad (\text{A8})$$

Expressed in terms of the relative amplitudes $\theta_s = \Omega_s/\Omega_0$, these parameters take the form $\alpha_{l,j,s} = \theta_s \alpha_{l,j}$, where $\alpha_{l,j} \equiv \alpha_{l,j,0}$. This mirrors the structure of the $\sigma_X \otimes \sigma_X$ gate coefficients from Eq. (7).

The second operator \hat{A}_2 for the LS gate has the form

$$\hat{A}_2 = i \sum_{s,s'=0}^{d-1} \sum_{j,k=1}^2 \chi_{jk;ss'}^{\text{LS}} |s_j\rangle\langle s_j| \times |s'_k\rangle\langle s'_k| \quad (\text{A9})$$

and can be obtained from the Magnus expansion formula (A3) for the Hamiltonian of the LS gate (14). The LS phases χ_{jk}^{LS} are defined in the main text in Eq. (19).

Appendix B: Multi-tone pulse shaping of the MS gate

In this Appendix we obtain the system, that we define in the main text in Eq. (26) and also discuss the important features of our multi-tone pulse shapes. The pulse function $g(t)$ defined in Eq. (B1) can be seen as the superposition of P tones, therefore defined as the multi-tone pulse shapes. The number of harmonics P and parameter n_{\min} define the range of detunings:

$$\mu_{\min} = 2\pi n_{\min}/\tau \leq \mu_p \leq \mu_{\max} = 2\pi(n_{\min} + P - 1)/\tau \quad (\text{B1})$$

These parameters are selected to position all motional modes within the range (μ_{\min}, μ_{\max}) , ensuring their efficient excitation.

Then, using the known technique from Ref. [49] we rewrite the decoupling condition (8) in terms of the amplitude vector $\vec{\Omega}$:

$$\alpha_{l,j}(\tau) = 0, \quad l = 1, \dots, N, \quad j = 1, 2 \Leftrightarrow \mathbf{M}\vec{\Omega} = 0, \quad (\text{B2})$$

where the matrix \mathbf{M} has the form

$$\mathbf{M}_{l,p} = \int_0^\tau \sin(\mu_p t) \sin\left[\omega_l\left(\frac{\tau}{2} - t\right)\right] dt. \quad (\text{B3})$$

The matrix \mathbf{M} is constructed by exploiting the anti-symmetry of the pulse function $g(t)$, which reduces the decoupling conditions to the simplified form given in Eq. (A6). The decoupling conditions can be expressed as a system of linear equations in terms of the amplitude vector $\vec{\Omega}$, solvable using standard linear algebra techniques. Lengthy but straightforward, one can obtain that the MS phases can be obtained in the form:

$$\chi_{jk}^{\text{MS}} = \vec{\Omega}^T \mathbf{D}_{jk} \vec{\Omega}, \quad (\text{B4})$$

where the matrices \mathbf{D}_{jk} are defined as

$$(\mathbf{D}_{jk})_{nm} = \sum_l \eta_{l,j} \eta_{l,k} \int_0^\tau dt_1 \int_0^{t_1} dt_2 \sin(\mu_n t_2) \sin(\mu_m t_1) \sin[\omega_l(t_1 - t_2)]. \quad (\text{B5})$$

Since the χ_{jk}^{MS} is a scalar, the equation can be symmetrized using the matrix $\mathbf{S}_{jk} = (\mathbf{D}_{jk} + \mathbf{D}_{jk}^T)/2$, see Eq. (24).

To find solutions non-sensitive in the first order to the motional modes drifts, we would also require that the derivatives of the phases with respect to secular frequencies be zero:

$$\frac{\partial \chi_{jk}^{\text{MS}}}{\partial \omega_l} = \vec{\Omega}^T \mathbf{Q}_{jk,l} \vec{\Omega} = 0, \quad (\text{B6})$$

for ions $j, k = 1, 2$ and motional modes $l = 1, \dots, N$. The matrices $\mathbf{Q}_{jk,l}$ have the form:

$$\mathbf{Q}_{jk,l} = \frac{\partial \mathbf{S}_{jk}}{\partial \omega_l} \quad (\text{B7})$$

The stabilization conditions in Eq. (B6) are $3N$ quadratic equations with multiple variables, which makes it difficult to find the solution numerically. Furthermore, some of the matrices $\mathbf{Q}_{jk,l}$ may be positive or negative definite, so that the stabilization condition cannot be satisfied exactly. Instead, we employ the projection method introduced in

Ref. [49]. The idea of this method is to reduce the derivative $\frac{\partial \chi_{jk}^{\text{MS}}}{\partial \omega_l}$ by projecting out M vectors that express the highest sensitivity to motional frequency drifts. From Eq. (B6) we conclude that the vectors to be projected out are the eigenvectors of matrices $\mathbf{Q}_{jk,l}$ with the highest magnitudes of their eigenvalues:

$$\mathbf{Q}_{jk,l} \vec{V}_{jk,l}^{(m)} = \lambda_{jk,l}^{(m)} \vec{V}_{jk,l}^{(m)}, \quad 1 \leq m \leq M, \quad (\text{B8})$$

where the eigenvalues $\lambda_{jk,l}^{(m)}$ are sorted in descending order of their magnitude: $|\lambda_{jk,l}^{(1)}| \geq |\lambda_{jk,l}^{(2)}| \geq \dots \geq |\lambda_{jk,l}^{(P)}|$. The higher the eigenvalue $\lambda_{jk,l}^{(m)}$, the more contribution of the vector $\vec{V}_{jk,l}^{(m)}$ to the derivative in (B6). Therefore, we project out the first M eigenvectors $\vec{V}_{jk,l}^{(m)}$ from each matrix $\mathbf{Q}_{jk,l}$. The final stabilization condition for phases χ_{jk}^{MS} can be written as

$$\mathbf{R}_\chi^T \vec{\Omega} = 0, \quad (\text{B9})$$

where matrix \mathbf{R}_χ is composed of the eigenvectors mentioned above as columns:

$$\mathbf{R}_\chi = \left[\vec{V}_{jk,l}^{(m)} \right]_{(jk,l,m) \in \mathcal{I}}, \quad (\text{B10})$$

where $\mathcal{I} = \{(jk, l, m) | jk = \{11, 12, 22\}, 1 \leq l \leq N, 1 \leq m \leq M\}$. The size of the matrix \mathbf{R}_χ is $P \times MN$ for each pair jk .

In addition to stabilization of MS phases, we also implement K -moment stabilization. This technique, employed in Ref. [49] enhances the gate robustness by suppressing the residual entanglement between electronic and motional states. Similarly to stabilization of χ_{jk}^{MS} phases the moment stabilization tries to set the first K derivatives of the $\alpha_{l,j}$ to zero:

$$\frac{\partial^k \alpha_{l,j}}{\partial \omega_l^k} = 0 \Leftrightarrow \mathbf{M}^{(k)} \Omega = 0, \quad (\text{B11})$$

where $\mathbf{M}^{(k)} = \partial^k \mathbf{M} / \partial \omega_l^k$. Using this relations, we construct the condition for residual entanglement stabilization in a form analogous to Eq. (B10):

$$\mathbf{R}_\alpha^T \vec{\Omega} = 0, \quad \mathbf{R}_\alpha = \left\{ \mathbf{M}^{(k)}, | k = 1, \dots, K \right\}. \quad (\text{B12})$$

The complete stabilization matrix used in the system of equations (26) is then given by the concatenation of the latter matrices $\mathbf{R} = [\mathbf{R}_\alpha; \mathbf{R}_\chi]$.

Appendix C: The existence of the solution for compensation of the single-qudit phases

The equation (10) for χ_{jk}^{MS} in the main text can be rewritten:

$$\chi_{jk}^{\text{MS}} = \sum_l \eta_{l,j} \eta_{l,k} \Theta_l, \quad (\text{C1})$$

$$\Theta_l = \int_0^\tau dt_1 \int_0^{t_1} g(t_1) g(t_2) \sin(\omega_l(t_1 - t_2)) dt_2. \quad (\text{C2})$$

Here θ_l depends on the pulse function $g(t)$, gate duration τ and

$$\begin{cases} \chi_{12}^{\text{MS}} = \sum_l \eta_{l,1} \eta_{l,2} \Theta_l = \chi, \\ \chi_{jj}^{\text{MS}} = \sum_l \eta_{l,j}^2 \Theta_l = 0, \quad j = 1, 2. \end{cases} \quad (\text{C3})$$

The solution of these system depends on the dimensionality of the $\vec{\Theta}$ and the number of the independent constraints. The number of parameters Θ_l matches the number of modes N , while the number of constraints is at most three. When the target ions are chosen symmetrically to the center of the ion chain, this leads to $\chi_{11}^{\text{MS}} = \chi_{22}^{\text{MS}}$, so there are

only two independent constraints. To guarantee the existence of the solution, we need $N \geq 2$, which can be achieved for any number of ions.

The key difference between multi-tone and amplitude modulations manifests in their ability to satisfy these compensation conditions. Given the solution $\vec{\Theta}_0$ to the compensation system (C3), we need to find a pulse function $g(t)$, that yields $\vec{\Theta} = \vec{\Theta}_0$ for $\vec{\Theta}$ given in Eq. (C2). Multi-tone modulation succeeds by placing the harmonics μ_p near all motional modes, enabling arbitrary Θ_l values. In contrast, the constant detuning μ in amplitude modulation does not allow to achieve arbitrary Θ_0 because the laser field interact mostly with the spectrally nearest modes. However, when attempting to stabilize against fluctuations in motional mode frequencies, the projection method constrains the subspace of viable solutions. Consequently, we cannot guarantee that a stabilized solution exists across all parameters. As demonstrated in the main text, we succeed in finding the shapes for parameter values typically used in experimental settings. While our algorithm fails to converge in broader parameter regions, alternative optimizer configurations may yield solutions for specific experimental requirements.

Appendix D: Native qudit gate representation of the cyclic shift \hat{X}_m^d

Any permutation of the qudit basis states can be performed by a series of resonant π -pulses between different level pairs, since this operation is equivalent to a swap. Therefore, to define a specific permutation, one needs to only specify the indices of levels being swapped in a certain sequence. In a real setup, though, it is only viable to use one of the qudit states for swapping, usually because it is spectrally separated from the rest. In the following, we call this state $|0\rangle$ or just 0 for brevity. Thus, the problem of cyclically shifting the whole basis by m , accounting for the restriction made above, can be reformulated as follows: provide a sequence of indices $1, 2, \dots, d-1$ in an array of d elements with indices $0, 1, \dots, d-1$ to be successively swapped with index 0, such that the array gets shifted by m units at the end.

To solve the problem, we first assume that $-d/2 < m \leq d/2$. If not, then redefine $m \rightarrow (m \bmod d) - d \cdot \theta((m \bmod d) - d/2)$. This is valid, because $\hat{X}_m^d = \hat{X}_{m+d}^d = \hat{X}_{-(d-m)}^d$. Second, any shift \hat{X}_m^d with $m < 0$ can be performed by simply reversing the sequence for $\hat{X}_{|m|}^d$, since pairwise swaps are their own inverses. Note that the sequence $[1, 2, \dots, d-1]$ realizes the shift \hat{X}_1^d in $d-1 = O(d)$ swaps. Technically, we can already build a working solution by applying the same unit shift m times, because $\hat{X}_m^d = \left(\hat{X}_1^d\right)^m$. However, this would require $O(md)$ native gates, which is undesirable for large $m \lesssim d/2$: the total cost scaling would be $O(d^2)$. In the following, we propose an algorithm that finds a suitable sequence with at most $3d/2 - 2 = O(d)$ swaps and with scaling independent of m .

Our proposition is a variation of the known "juggling" algorithm, which is based on *cycles*. Cycles are defined as index sequences of the form

$$a_n = (a_0 + mn) \bmod d, \quad (\text{D1})$$

with every element being unique. In other words, a cycle represents a closed loop of indices that are separated by m from each other. A cyclic shift of the whole array by m will shift each cycle by 1. Taking into account these observations, the construction of the juggling algorithm is straightforward: identify all cycles, then shift each cycle by 1 (see Fig. 9a). In our case, we are restricted to only using the 0-th index for swapping. That means that only the cycle $0, m, 2m, \dots$ can be shifted using the swap sequence $[m, 2m, \dots, d-m]$. For the rest of the cycles, we will use the 0-th element as a temporary buffer that will effectively prepend itself to the cycle. Then we will perform the same cyclic shift by 1, including the 0-th element. Afterwards, we swap the 0-th element with the first element of the cycle, achieving the desired shift (see Fig. 9b). To identify all cycles, note that the cycle length (the number of distinct indices in a cycle) can be calculated as

$$L = \frac{\text{lcm}(m, d)}{m} = \frac{d}{\text{gcd}(m, d)}, \quad (\text{D2})$$

which is the same for all cycles. The number of cycles is therefore $g = d/L = \text{gcd}(m, d)$. Each index $0, 1, \dots, g-1$ belongs to a different cycle, because the separation between different indices in the same cycle has to be divisible by g . Therefore, all cycles are generated by the first g indices. In conclusion, the swap sequence can be written as follows:

$$\begin{aligned} & [m, 2m, \dots, d-m, \\ & 1, m+1, 2m+1, \dots, d-m+1, 1, \\ & 2, m+2, 2m+2, \dots, d-m+2, 2, \\ & \dots, \\ & g-1, m+(g-1), 2m+(g-1), \dots, d-m+(g-1), g-1]. \end{aligned} \quad (\text{D3})$$

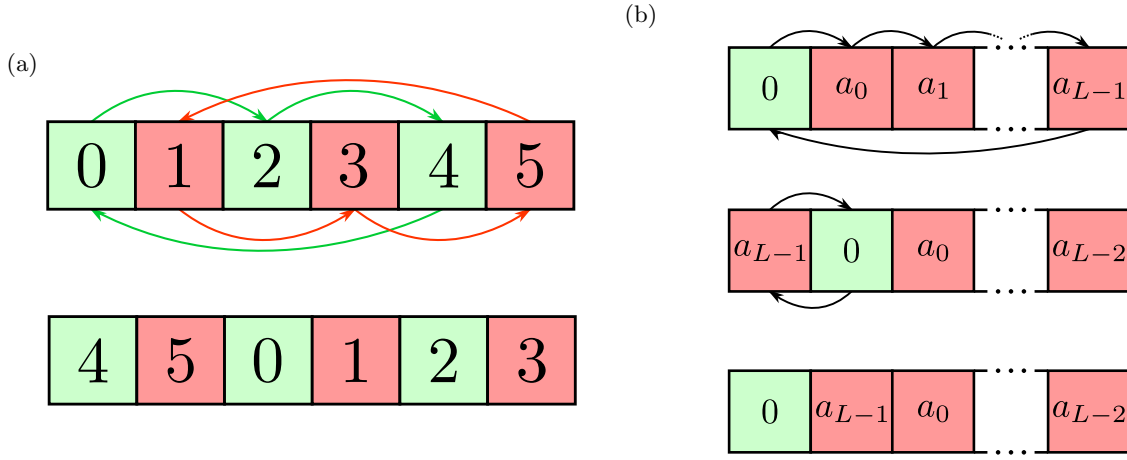


Figure 9: (a) The original juggling algorithm for $d = 6, m = 2$. The arrows represent shifts within each cycle. (b) Shifting an arbitrary cycle using element 0 as a buffer for swaps. Arrows represent shifts experienced by every element at the end of the respective cyclic rotation. The pairwise swaps still include 0.

The number of swaps can be calculated exactly: the first cycle requires $L - 1$ swaps, the rest $g - 1$ cycles require $L + 1$ swaps because of the buffer index 0. Therefore, the total number of swaps is

$$N = (L - 1) + (g - 1)(L + 1) = d + \gcd(m, d) - 2. \quad (\text{D4})$$

The highest value that $\gcd(m, d)$ can take is $d/2$, so the worst-case upper bound on the number of swaps is $3d/2 - 2 = O(d)$.

Appendix E: Spin-echo sequence for embedded qubits

The spin-echo sequence of type (c) comprises $d^2/2$ two-particle gates, and thus its complexity increases rapidly with the qudit dimension d . It is therefore desirable to identify scenarios in which this reduced gate configuration can be advantageously applied. As discussed in Sec. V, such a gate enables the realization of two-qubit operations within embedded-qubit architectures. In the following, we provide a formal proof of this statement.

Consider implementing the light-shift (LS) gate on a pair of qudits labeled Q_1 and Q_2 , each of dimension d . We employ the mapping $|j\rangle_Q \leftrightarrow |\text{bin}_2(j)\rangle_{q_1 \dots q_n}$, which embed n qubits into a single qudit with $d = 2^n$, and $\text{bin}_2(j)$ is the 2-binary representation of j . For a system of two qudits, we denote the embedded qubits by q_{ij} , where the index i specifies the qudit Q_i in which the qubit is encoded, and j labels the qubit itself. Our goal is to implement a two-qubit entangling operation of the form $\sigma_Z \otimes \sigma_Z$:

$$\text{ZZ}_{q_1, q_2}(\chi) := \exp(i\chi \sigma_Z^{q_1} \otimes \sigma_Z^{q_2}), \quad (\text{E1})$$

Here, $\sigma_Z^{q_i}$ denotes the Pauli- Z operator acting on the qubit q_i . As a first step, we perform a transpilation of $\sigma_Z^{q_i}$ into the corresponding qudit operators. Consider a 2×2 unitary \mathcal{U} acting within the subspace of the qubit q_i with an identity operation acting in the remaining space of a qudit [33]:

$$\mathcal{U}_{q_i} = \sum_{(\alpha, \beta)} \mathcal{U}^{\alpha, \beta}, \quad (\text{E2})$$

where $\mathcal{U}^{\alpha, \beta}$ means 2×2 unitary that acts in the subspace of the summation is made over all pairs (α, β) that satisfy:

$$\begin{aligned} \text{bin}_2(\alpha) &= x_1 \dots x_{i-1} 0 x_{i+1} \dots x_n, \\ \text{bin}_2(\beta) &= x_1 \dots x_{i-1} 1 x_{i+1} \dots x_n, \end{aligned} \quad (\text{E3})$$

where $x_1 \dots x_{i-1} x_{i+1} \dots x_n$ are all possible bitstrings of length $n - 1$. These condition can be simplified

$$\beta - \alpha = 2^{n-i}. \quad (\text{E4})$$

The Eq. (E2) can be used for σ_Z gate. Consider the σ_Z gate on the last qubit \mathbf{q}_n , using the relation (E4):

$$\sigma_Z^{\mathbf{q}_n} = \sum_{l=0}^{d/2-1} \sigma_Z^{2l, 2l+1}, \quad (\text{E5})$$

where $\sigma_Z^{i,j} = |i\rangle\langle i| - |j\rangle\langle j|$. One can substitute these relation to Eq. (E1) for $\text{ZZ}_{\mathbf{q}_{1n}\mathbf{q}_{2n}}$ and obtain:

$$\text{ZZ}_{\mathbf{q}_{1n}\mathbf{q}_{2n}}(\chi) = \exp\left(i\chi \sum_{l,m=0}^{d/2-1} \sigma_Z^{2l, 2l+1} \otimes \sigma_Z^{2m, 2m+1}\right). \quad (\text{E6})$$

Since the operator inside the exponent is diagonal in the computational basis, we can obtain that states acquire the state-dependent phase:

$$\text{ZZ}_{\mathbf{q}_{1n}\mathbf{q}_{2n}}(\chi) : |ss'\rangle \rightarrow e^{i\psi_{ss'}} |ss'\rangle, \quad (\text{E7})$$

where $\psi_{ss'}$:

$$\psi_{ss'} = \begin{cases} \chi, & s - s' \mid 2, \\ -\chi, & s - s' \nmid 2. \end{cases} \quad (\text{E8})$$

By comparison with the spin-echo sequence of type (c), given in Eq. (42), it is evident that the two are equivalent up to a global phase. To realize the embedded ZZ-gate on other qubits, one can swap the qudits inside one qudit before and after the spin-echo sequence. Such swaps can be realized using only single-qudit gates.
